A Human Decision Making Model for Bulldozer 3D Blade Control

Samuel R. Dekhterman[1], Marius Juston[1], William R Norris[1], Dustin Nottage[1], and Ahmet Soylemezoglu[1]

[1]Affiliation not available

August 06, 2024

Posted on 6 Aug 2024 — CC-BY 4.0 — https://doi.org/10.36227/techrxiv.172296516.63132907/v1 — e-Prints posted on TechRxiv are preliminary reports that are not peer reviewed. They should not b...

A Human Decision Making Model for Bulldozer 3D Blade Control

Samuel R. Dekhterman, Marius Juston, William R. Norris, Dustin Nottage, Ahmet Soylemezoglu

***Abstract*—This paper derives a set of bulldozer dynamics to test a three-dimensional (3D) blade controller. This work was motivated by a desire to mimic how a human operator would control a bulldozer blade to build an autonomous system control module and by the lack of existing work on 3D bulldozer blade control. To that end, three-dimensional surface-to-track and surface-to-blade dynamics were derived to test the proposed 3D bulldozer blade controller in simulation. The track dynamics included considerations for track slip, while the blade dynamics accounted for non-symmetric mounds in front of the blade. The 3D bulldozer blade control effort was implemented using fuzzy logic to mimic a human operator's nonlinear modes of blade control, thereby following a Human Decision Making Model (HDMM). The inputs to the main portion of the control effort were the yaw, pitch, and roll errors between the blade's current orientation and the desired orientation. Accordingly, the outputs were the blade's yaw, pitch, and roll velocities. The pitch error, in particular, was tied to a separate fuzzy controller that outputted the desired cutting depth depending on the observed soil type, against tying back to the HDMM.**

***Index Terms*—3D bulldozer dynamics, 3D blade control, fuzzy logic, Lyapunov stability, operator model.**

I. Introduction

A bulldozer is a highly versatile piece of earth-moving equipment that can be used for clearing, backfilling, finishing surfaces, etc. [1] [2] [3]. Bulldozer applications are seen across various industries, including mining, construction, and agriculture [4]. Given both the complexity of operation and value proved by bulldozers, there has been longstanding interest in automating bulldozer operation to reduce training time/labor costs [5].

The study in [6] derived a set of forward kinematic equations to move from a Dual RTK GPS position module in the cabin of a bulldozer to the bulldozer's cutting edge. Knowledge of the blade's position enabled the implementation of a virtual spring-damped controller that actuated the blade's cutting edge towards a desired design surface by actuating the blade's pitch joint. Testing was conducted outdoors, where the controller achieved around five centimeters of error on average when leveling a surface.

The authors of [7] extended the work in [6] to consider the vehicle's base and main joint's orientation when controlling the blade. This consideration was made to focus the control effort on the actuation of a hydraulic cylinder that changed the blade's pitch. With this change, [7] improved outdoor leveling accuracy to within an average of four centimeters of error from the desired design surface.

The authors of [7] expanded on their work in [8] to integrate limitations around a dozer's hydrostatic transmission and the hydraulic flow rate associated with the actuation for the dozer's pitch joint. These limitations were combined with the joint movement control in the authors' previous work. Limits on the move-base velocity were established based on the actuator's flow rate for the blade's pitch joint. Further, move-base acceleration restrictions reduced blade oscillation.

The authors of [7] and [8] continued their research in [9], focusing again on pitch blade control. Mononen and co.'s innovation in [9] was the use of LiDAR to gain elevation information about the dozing surface. The elevation information in front of the bulldozer was locally normalized into a representative surface. A design surface was then established relative to this representative surface. The control effort was separated into two stages, soil cutting/loading and soil pushing/carrying.

Separate from PID control, other works like [10] incorporated nonlinear model predictive control (NMPC) of a bulldozer blade's pitch. [10] used a far more detailed model of a bulldozer's hydraulics than the authors' later work in [7], [8], and [9].

Another controller type recently investigated in the literature was learning-from-demonstration [11], [12]. In [12], a deep convolutional neural network was trained to control a bulldozer using video recordings of an expert operator. While the paper demonstrated excellent performance against real-world operators, the authors of this paper had reservations about the robustness of that controller across different weather conditions, lighting conditions, and environments.

A more traditional control type, mainly fuzzy logic control, was used in [13] to determine how much force should be applied to a bulldozer blade. The work in [14] also used a fuzzy control to actuate a bulldozer blade along a single plane. That controller took in the engine torque, body angle, and the relative angle of the blade to the body for a known driving surface angle. These were then used to determine

Samuel R Dekhterman is in the Department of Industrial and Enterprise Systems Engineering, University of Illinois Urbana-Champaign, IL, 61801, USA e-mail: srd2@illinois.edu.

Marius Juston is in the Department of Industrial and Enterprise Systems Engineering, University of Illinois Urbana-Champaign, IL, 61801, USA e-mail: mjuston2@illinois.edu.

William R Norris is a Clinical Associate Professor in the Department of Industrial and Enterprise Systems Engineering, University of Illinois Urbana-Champaign, IL, 61801, USA e-mail: wrnorris@illinois.edu.

Dustin Nottage and Ahmet Soylemezoglu are in the Construction Engineering Research Laboratory, U.S. Army Corps of Engineers Engineering Research and Development Center, IL, 61822, USA.

This research was supported by the U.S. Army Corps of Engineers Engineering Research and Development Center, Construction Engineering Research Laboratory and conducted by the Center for Autonomous Construction and Manufacturing at Scale at the University of Illinois Urbana-Champaign.

Manuscript received April 19, 2024; revised August 16, 2024.

the desired change in the blade's pitch. Fuzzy control was chosen to replicate the control actions taken by an expert who was observed to make several minor adjustments during the bulldozer operation. The study in [14] examined how the control action could be adapted depending on whether the mission was leveling or clear. Given the flexibility of this control type, it was chosen for the proposed controller.

Some papers have investigated the use of Finite Element Analysis to model the forces and joints associated with a bulldozer blade pushing/ cutting into soil [15] [16]. Alternatively, [17] investigated a soil-centric Discrete Element Method of the same phenomena. While highly accurate, these methods were considered overly complicated for the fast-paced controller design the authors were interested in. As such, the authors decided to extend the simple 2D blade model presented in [18] to 3D.

Bulldozer models such as the ones in [18] and [19] considered most of the dynamics of the systems between the engine and tracks. Some models focused more on the bulldozer track, such as [20]. Given the complexity of these models, the authors opted for a modified version of the track dynamics presented in [21]. These modifications of [21] entailed expanding the paper's dynamics from 2D to 3D surfaces.

This paper proposes a fuzzy blade controller that uniquely actuates the yaw, pitch, and roll of a bulldozer's blade to better align with the Human Decision Making Model (HDMM) of an expert bulldozer operator. This is unique as all work the authors found on the subject only provided pitch blade control. The use of fuzzy logic enabled both the blade control to adapt to an artificially observed soil type and more straightforward safety validation than the machine learning controller in [12]. The simulation used to test the controller incorporated a unique set of 3D bulldozer dynamics.

The remainder of the paper is structured as follows: Section II derives the set of dynamics considered in the bulldozer simulation. Section III explains the proposed control effort and provides a stabiltiy proof of the controller. Section IV establishes the experiment design. Section V examines the experimental results achieved using the proposed controller in simulation. Finally, Section VI contains concluding thoughts and recommendations for future work.

II. Simulation Dynamics

The following set of 3D dynamics were employed to model a bulldozer in simulation. The 3D track dynamics were built of the 2D track dynamics presented in [21].

For this model, τ was an array containing the drive wheel torques for the left and right tracks, τ_L and τ_R, respectively. Namely, $\tau = [\tau_L, \tau_R]^T$. In addition, $q = [X, Y, Z, A, B, \Gamma]^T$ was an array containing the vehicle's X, Y, Z positions, and the orientations about the x, y, and z axes A, B, Γ, respectively. $\dot{q} = [\dot{X}, \dot{Y}, \dot{Z}, \dot{A}, \dot{B}, \dot{\Gamma}]^T$ was an array containing the vehicle's $\dot{X}$, $\dot{Y}$, $\dot{Z}$ linear speeds, and the angular velocities about the x, y, and z axes $\dot{A}, \dot{B}, \dot{\Gamma}$, respectively. Both q and $\dot{q}$ were in the global reference frame. There was also a local body reference frame and a blade reference frame. The blade frame x, y, and z axes originating at the center of mass of the unloaded bulldozer with coordinates x, y, and z. The blade frame x, y, and z axes originate at the center bottom of the blade with coordinates x_b, y_b, and z_b.

To rotate from the global to the local frame (sub-scripted gl), the map R_{gl} was used such that $c(\cdot)$ was the cosine of a given angle and $s(\cdot)$ was the sine of a given angle. Observe, that R_{gl} is orthonormal, the proof of which is left to the reader; as such, the inverse of R_{gl} is equivalent to its transpose. A fact that was helpful when transforming from the local to the global frame (sub-scripted lg); $R_{gl}^T = R_{lg}$. R_{bl} denoted the transformation matrix used to move from the blade to the local body frame (sub-scripted bl). Note that, equation (1) was taken from [22] and that the columns of R_{lg} in equation (2), R_{lg_X}, R_{lg_Y}, and R_{lg_Z} will be used on subsequent pages.

$$R_{gl} = \begin{bmatrix} c_B c_\Gamma & s_A s_B c_\Gamma - c_A s_\Gamma & c_A s_B c_\Gamma + s_A s_\Gamma \\ c_B s_\Gamma & s_A s_B s_\Gamma + c_A c_\Gamma & c_A s_B s_\Gamma - s_A c_\Gamma \\ -s_B & s_A c_B & c_A c_B \end{bmatrix}. \quad (1)$$

$$R_{gl}^T = R_{lg} = \begin{bmatrix} R_{lg_X} & R_{lg_Y} & R_{lg_Z} \end{bmatrix}. \quad (2)$$

The vehicle's local body linear and angular velocities were calculated using R_{gl} and the vehicle's global linear and angular velocities in equation (3). In equation (3) $\dot{x}$ was the local x velocity, $\dot{y}$ was the local y velocity, $\dot{z}$ was the local z velocity, $\dot{\alpha}$ was the angular velocity about the local x-axis, $\dot{\beta}$ was the angular velocity about the local y-axis, and $\dot{\gamma}$ was the angular velocity about local z-axis.

$$\begin{bmatrix} \dot{x} \\ \dot{y} \\ \dot{z} \end{bmatrix} = R_{gl} \begin{bmatrix} \dot{X} \\ \dot{Y} \\ \dot{Z} \end{bmatrix}, \quad \begin{bmatrix} \dot{\alpha} \\ \dot{\beta} \\ \dot{\gamma} \end{bmatrix} = R_{gl} \begin{bmatrix} \dot{A} \\ \dot{B} \\ \dot{\Gamma} \end{bmatrix}. \quad (3)$$

The x coordinate of the Instantaneous Center of Rotation of the vehicle in its local body frame was x_{ICR}. If $\dot{\gamma}$ was zero, then x_{ICR} was undefined and thus set to zero. Since a bulldozer is a differential steer vehicle, x_{ICR} was determined using equation (4) [23] and bounded between $-l/2$ and $l/2$ where l was the track length, in line with [24].

$$x_{ICR} = -\dot{y}/\dot{\gamma}. \quad (4)$$

The left and right local x-axis velocities of the tracks were denoted by the v_{tL} and v_{tR}, equations (5) and (6) respectively, [25]. In equations (5) and (6) b was the distance between the center of the tracks (track gauge) and both track velocities were saturated using the maximum vehicle velocity, s_{max}.

$$v_{tL} = \dot{x} - b/2 * \dot{\gamma}. \quad (5)$$

$$v_{tR} = \dot{x} + b/2 * \dot{\gamma}. \quad (6)$$

The longitudinal friction distribution was denoted by the r_l in equation (7) where μ_l was the coefficient of longitudinal resistance, m was the mass of the unloaded vehicle, and g was Earth's gravitation acceleration.

$$r_l = \mu_l * m * g/2. \quad (7)$$

Equation (8) was used to determine the track friction, $G(\cdot)$, where F was the applied force, f was the rolling friction, and $\dot{x}$ was the vehicle's velocity along/about the local body axis the force is applied [25]. As such, the function had conditions for whether the bulldozer was moving and overcame static

friction, whether the bulldozer was not moving and the track force was less than static friction, or whether the bulldozer was not moving and the track force was greater than static friction.

$$G(F, f, \dot{x}) = \begin{cases} -f * sign(\dot{x}) & \dot{x} \neq 0 \\ -F & \dot{x} = 0 \text{ and } |F| \leq f \\ -f * sign(F) & \text{otherwise.} \end{cases} \quad (8)$$

R_{lL} and R_{lR} denoted the left and right longitudinal resistance forces. The equations for each were equations (9) and (10), with r being the radius of the drive wheels driving each of the tracks.

$$R_{lL} = G(\tau_L/r, r_l, v_{tL}). \quad (9)$$

$$R_{lR} = G(\tau_R/r, r_l, v_{tR}). \quad (10)$$

The longitudinal resistance forces were then compiled in the R_l array, $R_l = [R_{lL}, R_{lR}]^T$. The lateral friction distribution equation, equation (11) was denoted by the fy. In equation (11), μ_t was the coefficient of lateral resistance.

$$fy = \mu_t * m * g/l. \quad (11)$$

Equation (12) was used to compute the lateral friction force, Fy.

$$Fy = -2 * sign(\dot{y}) * fy * |x_{ICR}|. \quad (12)$$

The resistive moment, m_r, was determined using equation (13).

$$m_r = 2 * fy * (l^2/4 - x_{ICR}^2). \quad (13)$$

The turning moment, M, was computed using equation (14), [21].

$$M = ((\tau_R/r + R_{lR}) - (\tau_L/r + R_{lL})) * b/2. \quad (14)$$

Equation (15) evaluated the moment of turning resistance, M_r.

$$M_r = G(M, m_r, \dot{\gamma}). \quad (15)$$

The modified versions of the blade forces from [18] were included in the simulation. Additionally, [18] assumed the bulldozer blade was a plate. The simulation maintained that assumption but altered the area of soil loaded on the plates and thus, the volume of the mound pushed by the bulldozer. For that new area, the roll of the blade relative to the slope α_{rel} was used, see Figure 1. In Figure 1, the width of the blade B_1 and the desired minimum cutting depth, h_p, were also known. Thus, the cutting area was computed using equation (16) where the area of a right triangle with a height of H_1 and a base of B_1 was summed with the area of a parallelogram of height h_p and length l_p where l_p was the hypotenuse of the right triangle.

$$Area_{cut} = \frac{1}{2} B_1 H_1 + l_p * h_p. \quad (16)$$

H_1 was computed using equation (17) and definition of the tangent function.

$$\tan(|\alpha_{rel}|) = \frac{H_1}{B_1} \implies H_1 = B_1 \tan(|\alpha_{rel}|). \quad (17)$$

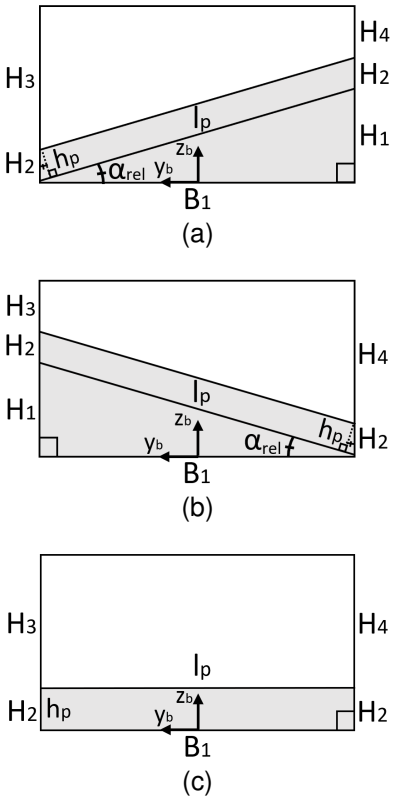

Fig. 1. Loading on bulldozer blade for an uneven load where the gray segments are the parts of the blade cutting into the soil. (a) corresponds to a positive relative roll angle, (b) corresponds to a negative relative roll angle, and (c) corresponds to a relative roll angle of zero.

The right triangle's hypotenuse was computed using the definition of the cosine function, equation (18).

$$cos(|\alpha_{rel}|) = B_1/l_p \implies l_p = B_1 \sec(|\alpha_{rel}|). \quad (18)$$

H_2, the height of the side of the parallelogram was computed using the definition of the cosine in equation (19), as applied to the right triangle present in Figure 2.

$$\cos(|\alpha_{rel}|) = \frac{h_p}{H_2} \implies H_2 = h_p \sec(|\alpha_{rel}|). \quad (19)$$

The left, H_3, and right, H_4, sides of the exposed area of the plate where computed using equations (20) and (21), such that H was the total height of the blade and equation (22) was the sign function.

$$H_3 = H - H_2 + sgn(\alpha_{rel}) \frac{H_1}{2} - \frac{H_1}{2}. \quad (20)$$

$$H_4 = H - H_2 - sgn(\alpha_{rel}) \frac{H_1}{2} - \frac{H_1}{2}. \quad (21)$$

$$sgn(x) = \begin{cases} 1 & x > 0 \\ 0 & x = 0 \\ -1 & x < 0. \end{cases} \quad (22)$$

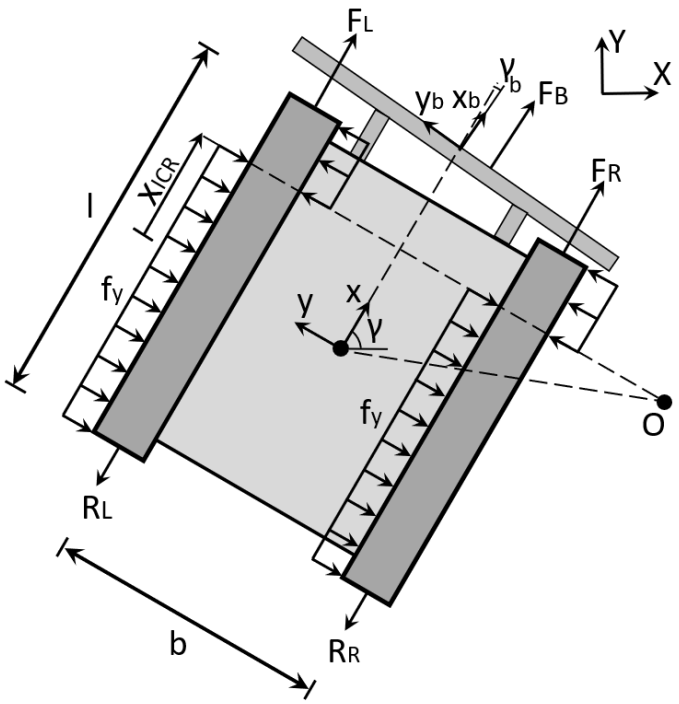

Fig. 2. The 2D track forces on the bulldozer when the z-axes for the world frame, track frame, and blade frame all point in the same direction.

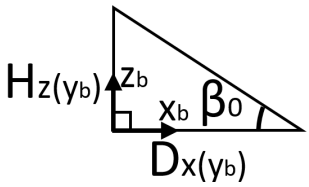

Fig. 3. The relation between the height, $H_z(y_b)$, and depth, $D_x(y_b)$, of the pile for a given natural soil slope angle, β_0.

The heights along the exposed area of the plate, $H_z(y_b)$, were computed using equation (23) where $y_b \in [-B_1/2, B_1/2]$.

$$H_z(y_b) = \frac{-H_3 + H_4}{B_1} y_b + \frac{H_3 + H_4}{2}, \tag{23}$$

$$= -sgn(\alpha_{rel}) \tan(|\alpha_{rel}|) y_b + H_m. \tag{24}$$

Given $H_z(y_b)$, $D_x(x_b)$, the depth of the mount at position x_b along the width of the blade was computed using the definition of the tangent where β_0 was the natural slope angle of the soil as seen in Figure 3 and derived in equations (25).

$$\tan(\beta_0) = \frac{H_z(y_b)}{D_x(y_b)} \implies D_x(y_b) = H_z(y_b) \cot(\beta_0). \tag{25}$$

The volume of the mound being pushed in front of the plate V was approximated using equations (26) - (29), where k_m was the fullness coefficient of the soils. The volume was assumed to fill linearly throughout the distance, d_{fill}.

$$V = k_m \int_{-B_1/2}^{B_1/2} \frac{1}{2} D_x(y_b) H_z(y_b) dy_b, \tag{26}$$

$$= k_m \int_{-B_1/2}^{B_1/2} \frac{1}{2} (H_z(y_b) \cot(\beta_0)) H_z(y_b) dy_b, \tag{27}$$

$$= \frac{k_m \cot(\beta_0)}{2} \int_{-B_1/2}^{B_1/2} H_z(y_b)^2 dy_b, \tag{28}$$

$$= \frac{k_m \cot(\beta_0)}{2} \left[\frac{\tan^2(|\alpha_{rel}|)}{12} B_1^3 + H_m^2 B_1 \right]. \tag{29}$$

Equation (30) determined G_t, the weight of the mound in front of the blade, such that γ_0 was the density of the soil, k_s was the soil looseness coefficient.

$$G_t = V * \gamma_0 / k_s. \tag{30}$$

Figure 5 visualizes the two forces acting upon the blade. F_1, the soil-shear force, was evaluated using equation (31) where k_b was the soil-cutting force per unit area and $Area_{cut}$ was defined as in equation (16).

$$F_1 = Area_{cut} * k_b. \tag{31}$$

Equation (32) computed, F_2, the pushing resistance force for the mound in front of the blade where μ_{ss} was the intra soil-to-soil rolling friction.

$$F_2 = G_t * \mu_{ss}. \tag{32}$$

The overall blade push-back force, F_b, was thus computed with equation (33).

$$F_b = -F_1 - F_2. \tag{33}$$

Equation (34) was used to compute the y_b-coordinate of the centroid of a trapezoid, y_c, as seen in Figure 4. In equation (34) and Figure 4, B_1 was the base of the trapezoid, D_1 was

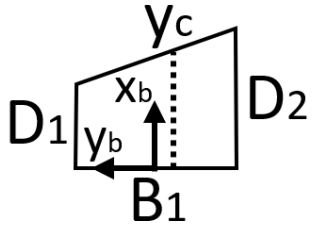

Fig. 4. A representation of the pile's trapezoidal depth with base B_1 and side lengths D_1 and D_2.

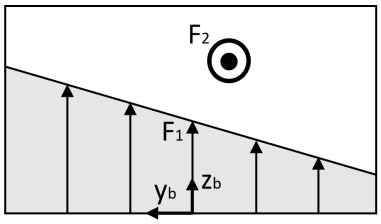

Fig. 5. A representation of the 2D blade forces on the bulldozer. F_1 denotes the soil sheer force across the bottom portion of the blade and F_2 indicates the pushing resistance force against the soil mound.

the smaller depth of the trapezoid, D_2 was the larger depth of the trapezoid.

$$y_c = \frac{D_1 + 2D_2}{3(D_1 + D_2)} B_1 - \frac{B_1}{2}. \tag{34}$$

The local y blade coordinate of the centroid of the trapezoidal pile, y_{c2}, was computed using equation (34) with $D_1 = D_x(-B_1/2)$ and $D_2 = D_x(B_1/2)$. Equation (34) was also used to find the local y blade coordinate where F_1 acted, y_{c1}, with $D_1 = H_2$ and $D_2 = H_1 + H_2$.

y_{c1} and y_{c2} were then used in equation (35) to determine the local blade z-axis resistive moment from the blade forces.

$$M_b = y_{c1}F_1 + y_{c2}F_2. \tag{35}$$

A non-holonomic constraint imposed on the vehicle in [21] limited the vehicle movement in line with equation (4), which is equivalent to equation (36).

$$\begin{bmatrix} R_{lg_Y} \\ x_{ICR}R_{lg_Z} \end{bmatrix}^T \dot{q} = \mathcal{A}(q)\dot{q} = 0. \tag{36}$$

The matrix S that appears in equation (37) denotes a matrix whose columns were in the null space of $\mathcal{A}$.

$$S = \begin{bmatrix} R_{lg_X} & R_{lg_Y} \\ 0_{3x1} & R_{lg_Z}\frac{-1}{x_{ICR}} \end{bmatrix}. \tag{37}$$

The derivative of the S matrix with respect to time was denoted by the matrix $\dot{S}$, see equation (38). Up until this point the dependencies on time have been truncated in the above variables. Explicitly, A, B, Γ, and x_{ICR} all have a dependence on time.

$$\dot{S} = \begin{bmatrix} -s_B c_\Gamma \dot{B} - c_B s_\Gamma \dot{\Gamma} & -s_B s_\Gamma \dot{B} + c_B c_\Gamma \dot{\Gamma} \\ S_{21} & S_{22} \\ S_{31} & S_{32} \\ 0 & c_B x_{ICR}^{-1}\dot{B} - s_B x_{ICR}^{-2}\dot{x}_{ICR} \\ 0 & S_{52} \\ 0 & S_{62} \end{bmatrix}. \tag{38}$$

with the sub-components of $\dot{S}$ being separated out into equations (39) and (44).

$$S_{21} = (c_A s_B c_\Gamma + s_A s_\Gamma)\dot{A} + s_A c_B c_\Gamma \dot{B} - (s_A s_B s_\Gamma + c_A c_\Gamma)\dot{\Gamma}. \tag{39}$$

$$S_{31} = (c_A s_\Gamma - s_A s_B c_\Gamma)\dot{A} + c_A c_B c_\Gamma \dot{B} + (s_A c_\Gamma - c_A s_B s_\Gamma)\dot{\Gamma}. \tag{40}$$

$$S_{22} = (c_A s_B s_\Gamma - s_A c_\Gamma)\dot{A} + s_A c_B s_\Gamma \dot{B} + (s_A s_B c_\Gamma - c_A s_\Gamma)\dot{\Gamma}. \tag{41}$$

$$S_{32} = -(s_A s_B s_\Gamma + c_A c_\Gamma)\dot{A} + c_A c_B s_\Gamma \dot{B} + (c_A s_B c_\Gamma + s_A s_\Gamma)\dot{\Gamma}. \tag{42}$$

$$S_{52} = -c_A c_B x_{ICR}^{-1}\dot{A} + s_A s_B x_{ICR}^{-1}\dot{B} + s_A c_B x_{ICR}^{-2}\dot{x}_{ICR}. \tag{43}$$

$$S_{62} = s_A c_B x_{ICR}^{-1}\dot{A} + c_A s_B x_{ICR}^{-1}\dot{B} + c_A c_B x_{ICR}^{-2}\dot{x}_{ICR}. \tag{44}$$

The global forward track force matrix, B_t, was defined using equation (45).

$$B_t = \frac{1}{r}\begin{bmatrix} R_{lg_X} & R_{lg_X} \\ 0_{2x1} & 0_{2x1} \\ -c_A c_B b/2 & c_A c_B b/2 \end{bmatrix}. \tag{45}$$

C_t in equation (46) denoted the local body resistive track forces and moments.

$$C_t = \begin{bmatrix} R_{lL} + R_{lR} \\ Fy \\ 0_{2x1} \\ (M_r + (-R_{lL} + R_{lR}) * b/2) \end{bmatrix}. \tag{46}$$

C_b in equation (47) denoted the resistive blade forces in the local body's frame.

$$C_b = \begin{bmatrix} I & & 0_{3x3} & \\ & 0 & 0 & 0 \\ 0_{3x3} & 0 & 0 & 0 \\ & 0 & 0 & 1 \end{bmatrix} \begin{bmatrix} R_{bl} & 0_{3x3} \\ 0_{3x3} & R_{bl} \end{bmatrix} \begin{bmatrix} F_b \\ 0_{4x1} \\ M_b \end{bmatrix}. \tag{47}$$

C in equation (48) denoted all the global resistive forces and moments.

$$C = \begin{bmatrix} R_{lg} & 0_{3x3} \\ 0_{3x3} & R_{lg} \end{bmatrix}(C_t + C_b). \tag{48}$$

The P matrix in equation (49) represented the unloaded vehicle's gravitational potential energy.

$$P = \begin{bmatrix} 0_{2x1} \\ mg \\ 0_{3x1} \end{bmatrix}. \tag{49}$$

The moments of inertia about the local body x, y, and z axes of the unloaded bulldozer were computed using equations (50) - (52) respectively, where h was the height of the bulldozer [26].

$$I_x = \frac{m}{12}(b^2 + h^2). \tag{50}$$

$$I_y = \frac{m}{12}(h^2 + l^2). \tag{51}$$

$$I_z = \frac{m}{12}(b^2 + l^2). \tag{52}$$

Equation (53)'s $\mathcal{M}$ matrix was used to relate the mass and moment of inertia of the bulldozer to its linear and angular kinetic energy.

$$\mathcal{M} = \begin{bmatrix} m & 0 & 0 & 0 & 0 & 0 \\ 0 & m & 0 & 0 & 0 & 0 \\ 0 & 0 & m & 0 & 0 & 0 \\ 0 & 0 & 0 & I_x & 0 & 0 \\ 0 & 0 & 0 & 0 & I_y & 0 \\ 0 & 0 & 0 & 0 & 0 & I_z \end{bmatrix}. \tag{53}$$

The above matrices were related to the following Euler-Lagrange equation, equation (54), from [21].

$$\frac{d}{dt}\left(\frac{\partial L}{\partial \dot{q}}\right) - \frac{\partial L}{\partial q} + \mathcal{A}(q)\lambda = B_t(q)\tau + C(q, \dot{q}). \tag{54}$$

The Lagrangian from [21] was modified to have a nonzero gravitational potential energy and different kinetic energy, equation (55).

$$L = E_k - E_P \tag{55}$$

$$= \frac{1}{2}m(\dot{x}^2 + \dot{y}^2 + z^2) + \frac{1}{2}I_x\dot{\alpha}^2 + \frac{1}{2}I_y\dot{\beta}^2 + \frac{1}{2}I_z\dot{\gamma}^2 - mgZ. \tag{56}$$

Plugging the Lagrangian into the Euler-Lagrange equation resulted in equation (57) such that λ was chosen so that

$\mathcal{A}(q)\lambda = 0$ and $v = \left[\sqrt{\dot{x}^2 + \dot{y}^2 + \dot{z}^2}, \sqrt{\dot{\alpha}, \dot{\beta}, \dot{\gamma}}\right]$ was an array containing the combined local body velocities.

$$\mathcal{M}(\dot{S}v + S\dot{v}) + P + \mathcal{A}(q)\lambda = B_t(q)\tau + C(q, \dot{q}). \quad (57)$$

The following matrices in equations (58) - (62) were then transformed using S and $\dot{S}$ for the purpose of modifying equation (57).

$$\tilde{B} = S^T * B_t. \quad (58)$$
$$\tilde{C} = S^T * C. \quad (59)$$
$$\tilde{P} = S^T * P. \quad (60)$$
$$\tilde{\mathcal{M}} = S^T * \mathcal{M} * S. \quad (61)$$
$$\tilde{E} = S^T * \mathcal{M} * \dot{S}. \quad (62)$$

$\dot{v}$ was thus determined with equation(63), such that equation (63) was transformed from equation (57).

$$\dot{v} = \tilde{\mathcal{M}}^{-1}(\tilde{B} * \tau + \tilde{C} - \tilde{E} * v - \tilde{P}). \quad (63)$$

Finally, the updated global velocities were denoted by $\dot{q}_{new}$ and an integrated $\dot{v}$, v_{new}, in equation (64).

$$\dot{q}_{new} = S * v_{new}. \quad (64)$$

III. Controller Design

The control effort followed from a Human Decision Making Mode (HDMM) of an expert bulldozer operator. It was determined that an expert operator would use all axes of control, namely blade yaw, blade pitch, blade roll, driving direction, and driving speed when leveling a surface. It was assumed an expert would adjust their cutting depth depending on the soil type to not overly tax the machine.

The control effort was separated into two aspects: driving and blade control. The driving control was implemented using a PID controller where the error signal was the difference between the desired track torque and the actual track torque [27]. A K_P of one, K_I of zero, and K_D of zero were used to set a given driving command to the tracks. The blade control was implemented using fuzzy logic. The blade control effort was decomposed into determining an ideal cutting depth for the blade and actuating the hydraulics so the blade would approach the desired cutting depth and blade angles.

Fuzzy logic control establishes a set of crisp, numeric input and output variables similar to other control types [28] [29]. Fuzzy provides linguistic names for these input and output variables. Each input and output linguistic variable also has a set of associated linguistic values that describe their performance. The input and output linguistic values have membership functions that characterize the membership in each value between zero and one. For each input linguistic variable, the level of membership in each of its linguistic values, X_i, is determined using the associated crisp input, I_j, and membership function, $\mu_k(\cdot)$, see equation (65); it is common practice to overlap the input membership functions to better transition between control outputs.

$$X_i = \mu_k(I_j). \quad (65)$$

To determine the level of membership in a given output value, Y_k, a rule with an if-then structure is used to translate, often via equality, from the level of membership in a prescribed input linguistic value.

$$\text{If } X_k \text{ Then } Y_k.$$

Once each rule's level of membership in its output values is determined, an aggregation operation, as detailed in [30], is used to compute a singular output membership function, $\mu_s(\cdot)$. The authors used the maximization operation on the outputs of the rule base. That meant that only the highest level of membership in any output membership function was used before combining those membership functions as a singular function. The "center of mass" of this singular output membership function, equation (66), can be used to determine the final crisp output, O_l, along all values y_i in the output's range [31].

$$O_l = \frac{\sum_{i=1}^{n} \mu_s(y_i)(y_i)}{\sum_{i=1}^{n} \mu_s(y_i)}. \quad (66)$$

Take the fuzzy controller, tied to the HDMM, that determined the desired soil cutting depth based on the soil type for example. Its input variable was the artificially observed soil type. That linguistic variable was characterized by the linguistic values 'compact,' 'mixed,' or 'loose,' the trapezoidal membership functions for which are seen in Table I. The output membership functions of this controller characterized the desired cutting depth. The desired cutting depth had three linguistic values: "low", "lower", and "lowest." The membership functions associated with these output linguistic values were triangular, as tabulated in Table II. The rule base for this controller appears in Table III. The cutting depth was used to set a desired pitch angle for the blade given the length of the blade arm.

The blade angular velocity fuzzy controller used to actuate the hydraulic cylinder had three input linguistic variables: the yaw, pitch, and roll errors. Each of the errors was the difference between the desired angle and the current angle of the blade and each of the input variables had the same three linguistic values. Those three values were negative ('neg'), 'zero,' and positive ('pos'), the membership functions for which are present in Table IV. The output linguistic variables were the yaw, pitch, and roll angular velocities. As with the inputs, each output had the same linguistic values: negative ('neg'), 'zero,' and positive ('pos'). The membership functions associated with these output linguistic values are seen in Table V. The rule base for the blade angular velocity fuzzy controller is presented in Table VI. A fuzzy structure was chosen for the above two control tasks in order to mimic how a human operator could go about actuating a bulldozer in the field as in [14]. The selection of fuzzy over a standard PID for this portion of the controller effort was directly related to the HDMM. Having a set of linguistic rules provided a clearer mental framework for the authors to translate between reference materials created by expert operators that explained their decision processes associated with actuating a bulldozer [2] to the control effort.

A PID was used to represent the hydraulics used to move the blade. A K_P of $\frac{1}{550}$, K_I of zero, and K_D of zero were

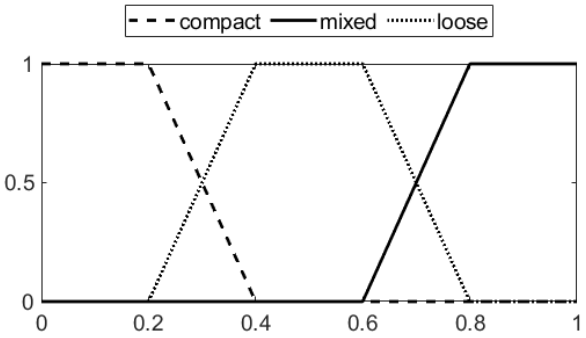

Fig. 6. The observed soil thickness linguistic values and membership functions.

TABLE I
THE OBSERVED SOIL THICKNESS LINGUISTIC VALUES AND MEMBERSHIP FUNCTIONS.

Linguistic Values	Membership Functions
compact	*trap*(0, 0, 0.2, 0.4)
mixed	*trap*(0.2, 0.4, 0.6, 0.8)
loose	*trap*(0.6, 0.8, 1, 1)

used to update the blade angles based on the angular velocities commanded by the angular velocity blade controller.

A. Stability Proof

The inputs of the blade angular velocity fuzzy controller were the roll, pitch, and yaw errors respectively, $x = \left[\alpha_{error}, \beta_{error}, \gamma_{error}\right]^T$ such that $x \in \mathbb{D}_1 \subset \mathbb{R}^3$ and $\mathbb{D}_1 : (-\pi, \pi] \times (-\pi, \pi] \times (-\pi, \pi]$. The domain $\mathbb{D}_1$ was set so that any angle less than or greater than $-\pi$ or π respectively were transformed into their equivalent $\pm 2\pi k \mid k \in \mathcal{Z}$ angle in the domain via a modulus operation. The output of the controller was equivalent to the change in the states, $y = \dot{x} = \left[\dot{\alpha}_{error}, \dot{\beta}_{error}, \dot{\gamma}_{error}\right]^T$ such that $\dot{x} \in \mathbb{D}_2 \subset \mathbb{R}^3$ where each dimension of $\mathbb{D}_2$ was between $[-1, 1]$. The blade angle controller transformed between x and $\dot{x}$ such that $\dot{x} = f(x)$. Each output for the controller given its associated input is seen in Figure 10. The shape of Figure 10 was influenced by the input membership functions sum of one at each point in each domain. For all inputs, engaging the zero input membership function, their outputs had a slope of negative ten. The output segments to the left and right of the section with a slope of negative ten were flat. Thus, for a $L = 10$ the controller was globally Lipschitz for all $x \in \mathbb{D}_1$, see [32] for details on the Lipschitz condition. Consider now the definition of Lyapunov stability, Theorem 1. from [33].

Theorem 1. Let $x = 0$ be an equilibrium point for and $D \subset \mathbb{R}^n$ be a domain containing $x = 0$. Let $V : D \to \mathbb{R}$ be a continuously differentiable function such that

$$V(0) = 0 \text{ and } V(x) > 0 \text{ in } D - \{0\}.$$

$$\dot{V}(x) \leq 0 \text{ in } D.$$

Then, $x = 0$ is stable.

The system's Lyapunov function was defined as $V(x) = x_1^2 + x_2^2 + x_3^2$. The first condition of **Theorem 1.** was satisfied for the chosen Lyapunov function as it was positive definite for all points aside from $(0, 0, 0)$ where $V(0) = 0$. Checking the second condition required the computation of $\dot{V}(x)$, see equations (67)- (70).

$$\dot{V}(x) = \sum_{i=1}^{n} \frac{\partial V(x)}{\partial x_i} \dot{x}_i, \tag{67}$$

$$= \frac{\partial V(x)}{\partial x_1} \dot{x}_1 + \frac{\partial V(x)}{\partial x_2} \dot{x}_2 + \frac{\partial V(x)}{\partial x_3} \dot{x}_3, \tag{68}$$

$$= 2x_1\dot{x}_1 + 2x_2\dot{x}_2 + 2x_3\dot{x}_3, \tag{69}$$

$$= 2(x_1\dot{x}_1 + x_2\dot{x}_2 + x_3\dot{x}_3). \tag{70}$$

TABLE II
THE INTENDED BLADE HEIGHT'S LINGUISTIC VALUES AND MEMBERSHIP FUNCTIONS.

Linguistic Values	Membership Functions
low	*tri*(-0.22, -0.20, -0.18)
lower	*tri*(-0.24, -0.24, -0.22)
lowest	*tri*(-0.32, -0.30, -0.28)

TABLE III
THE RULE-BASE OF THE FUZZY CONTROLLER THAT DETERMINED THE DESIRED BLADE CUTTING DEPTH BASED ON THE SOIL TYPE.

IF	THEN
Soil Type	**Depth**
compact	low
mixed	lower
loose	lowest

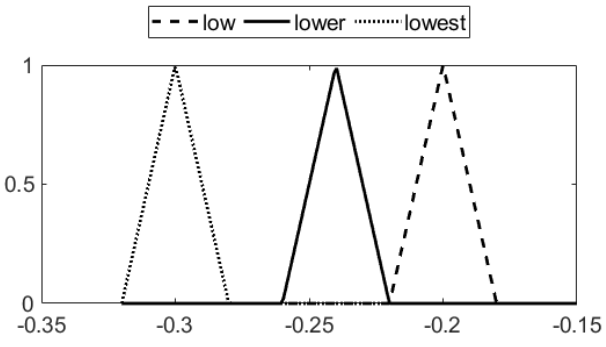

Fig. 7. The intended blade height's linguistic values and membership functions.

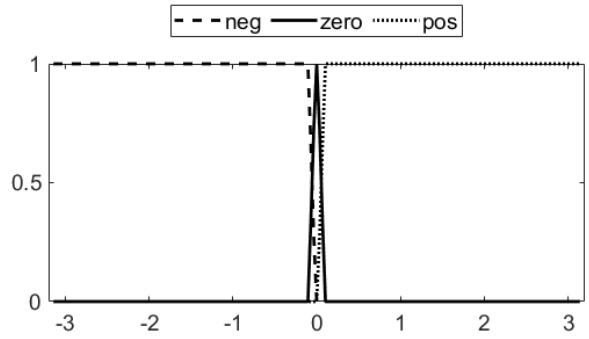

Fig. 8. Each angular error's linguistic values and membership functions.

TABLE IV
EACH ANGULAR ERROR'S LINGUISTIC VALUES AND MEMBERSHIP FUNCTIONS.

Linguistic Values	Membership Functions
neg	*trap*(-3.142, -3.142, -0.1, -0.01)
zero	*trap*(-0.1, -0.01, 0.01, 0.1)
pos	*trap*(0.01, 0.1, 3.142, 3.142)

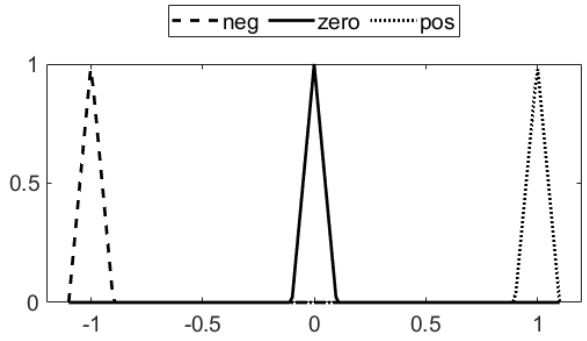

Fig. 9. Each angular velocity's linguistic values and membership functions.

The relationship between x_1 and $\dot{x}_1$ was the same as x_2 and $\dot{x}_2$ as well as x_3 and $\dot{x}_3$. This was due to the rules and membership function being the same for each error. For all xs where the 'zero' membership function had full membership, $\dot{x} = 0$. Thus, for those xs $x\dot{x} = 0$. For all the negative xs that had membership in the negative membership functions, $\dot{x} > 0 \implies x\dot{x} < 0$. Similarly, for all positive xs that had membership in the positive membership functions, $\dot{x} < 0 \implies x\dot{x} < 0$. Thus, the second condition of **Theorem 1.** was satisfied and the system was shown to be stable about its equilibrium point $x = 0$.

IV. EXPERIMENT DESIGN

All parameters used in the simulation can be found in Table VII. The bulldozer and blade parameters were those of a John Deere 650K LGP Tier 4 Final bulldozer with a standard blade [34]. The radius of the drive wheel and blade arm length were approximated from the pictures on [34]. The torques were assigned to near the maximum tractive torque the soil could maintain as per equation (71) where c_0 was the cohesion of the soil, m was the mass of the unloaded vehicle, g was the acceleration due to gravity, w was the width of the track, l was the length of the track, and β_0 was the natural slope angle of the soil [21].

$$\tau_{\max} = c_0 + \frac{m * \mathrm{g}}{wl} \tan(\beta_0). \tag{71}$$

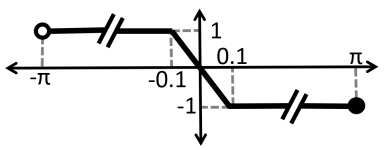

Fig. 10. The input to output map for each input-output pair of the blade angular velocity controller.

TABLE V
EACH ANGULAR VELOCITY'S LINGUISTIC VALUES AND MEMBERSHIP FUNCTIONS.

Linguistic Values	Membership Functions
neg	*tri*(-1.1, -1, -0.9)
zero	*tri*(-0.1, 0, 0.1)
pos	*tri*(0.9, 1, 1.1)

TABLE VI
THE FUZZY CONTROLLER RULE-BASE FOR SETTING THE ANGULAR VELOCITY BASED ON THE ANGULAR ERROR.

IF			THEN		
Yaw Er.	**Ptch Er.**	**Rl Er.**	**Yaw Vel.**	**Ptch Vel.**	**Rl Vel.**
neg zero pos			pos zero down		
	neg zero pos			pos zero down	
		neg zero pos			pos zero down

The lateral and longitudinal track rolling friction were taken from [35]. The soil-to-soil rolling friction, the soil sheering force per unit area, the bulk density of the soil (used to compute the gravity per cubic meter), the natural slope angle of the soil, and the soil cohesion were obtained from [36]. The fullness and looseness parameters of the soil were based on those in [37].

The test on the compact soil type used the following values: $\gamma_0 = 1480 * 9.81$, $k_m = 0.94$, $k_s = 1.06$, obs = 0.1. The test on the mixed soil type used the following values: $\gamma_0 = 1375 * 9.81$, $k_m = 0.92$, $k_s = 1.08$, obs = 0.5. The following values were used for testing on the loose soil type: $\gamma_0 = 1270 * 9.81$, $k_m = 0.90$, $k_s = 1.10$, and obs = 0.9.

The first two tests took inspiration from previous work in the literature [7] where a single axis was actuated while driving forwards. The first two tests were used to compare the effects of digging to different depths on a flat surface while driving forward by expanding the pitch piston, as per [7]. The third and fourth tests paired the depth-cutting portions of the control efforts with differences in surface roll and pitch slope angles, respectively. As well, the third and fourth tests added roll and yaw control efforts to their respective tests. The fifth test paired all of the elements seen in the third and fourth tests. Each control effort test had the vehicle drive forward for 0.3 meters in the simulation. This distance was chosen so the track surface pitch transitions mentioned in [38] did not have to be considered. The authors' MATLAB implementation of the equations can be found at https://github.com/AUVSL/nonCUI_bulldozer_blade_control.

V. EXPERIMENTAL RESULTS

The first test was to hit the desired depth for compact soil saw a Root Mean Squared Error (RMSE) of 0.156 meters with a starting error of 0.186 meters as depicted in Figure 11.

The second test demonstrated the control effort's ability to target a lower depth on a mixed soil type. This second test demonstrated an RMSE of 0.185 meters with a started error

TABLE VII
ALL PARAMETERS USED IN THE SIMULATION. BLANK VALUES ARE SEEN FOR PARAMETERS WHOSE VALUES CHANGE DEPENDING ON THE SELECTED SOIL TYPE.

Parameter	Value	Description
h	2.762	vehicle height [m]
l	2.349	track length [m]
w	0.7112	track width [m]
b	1.75	track gauge [m]
r	0.4	radius of drive wheel [m]
B_1	2.921	dozer blade width [m]
H	0.955	dozer blade height [m]
L	1.4	blade arm length [m]
d_{fill}	20.0	distance to fully fill mound [m]
s_{max}	133	maximum travel speed [m/s]
m	10156	mass of vehicle [kg]
g	9.81	gravitational acceleration[$\frac{m}{s^2}$]
τ_L	56000	left track torque [Nm]
τ_R	56000	right track torque [Nm]
μ_l	0.1	longitudinal tack friction coef.
μ_t	0.9	lateral track friction coef.
μ_{ss}	0.5	friction coef. between soil and soil
k_b	0.04	$\frac{\text{sheering resistance}}{\text{unit area}}$ (entering soil) [MPa]
β_0	38	natural slope angle of soil [degrees]
c_0	13	soil cohesion [kPa]
γ_0	-	gravity per cubic meter [$\frac{kN}{m^3}$]
α_{rel}	-	roll incline of the soil [degrees]
k_m	-	fullness degree coefficient of soil
k_s	-	loose degree coefficient of soil
obs	-	perceived fullness coefficient

of 0.226 meters. The full lowering control effort is seen in the starting linear segments in the top plot of Figure 11. A smooth transition towards the final depth was demonstrated in both with a longer tail on the compact soil type, as a smaller digging depth was desirable.

The third test attempted to control both the depth and roll of the blade on a surface with a roll of -0.2 radians and a loose soil type. The controller experienced RMSEs of 0.230 meters and 0.079 radians with starting errors of 0.286 meters and 0.200 radians in regards to the depth and roll errors, respectively. The roll error for this test is seen in the second plot from the top of Figure 11. The error was negative as the roll component as the controller was seeking to level a negatively sloped surface.

The fourth test was similar to the third test where the soil type was again loose and there was a depth component to the control effort. Unlike the third test, however, the fourth test replaced the -0.2 radian roll of the surface with a -0.2 radian pitch and replaced the roll portion of the control effort with a yaw portion. This test saw depth and yaw blade RMSEs of 0.219 meters and 0.085 radians. The corresponding depth and yaw starting errors were 0.285 meters and 0.200 radians.

Test five examined the depth, yaw, and roll control efforts all at once. This test was on a surface with a loose soil type, a pitch of 0.2 radians, and a roll of 0.2 radians. The fifth test saw RMSEs of 0.224 meters, 0.082 radians, and 0.082 radians of depth, roll, and yaw error, respectively. The starting errors were the same as in previous tests with 0.286 meters of depth error, 0.200 radians of roll error, and 0.200 radians of pitch error.

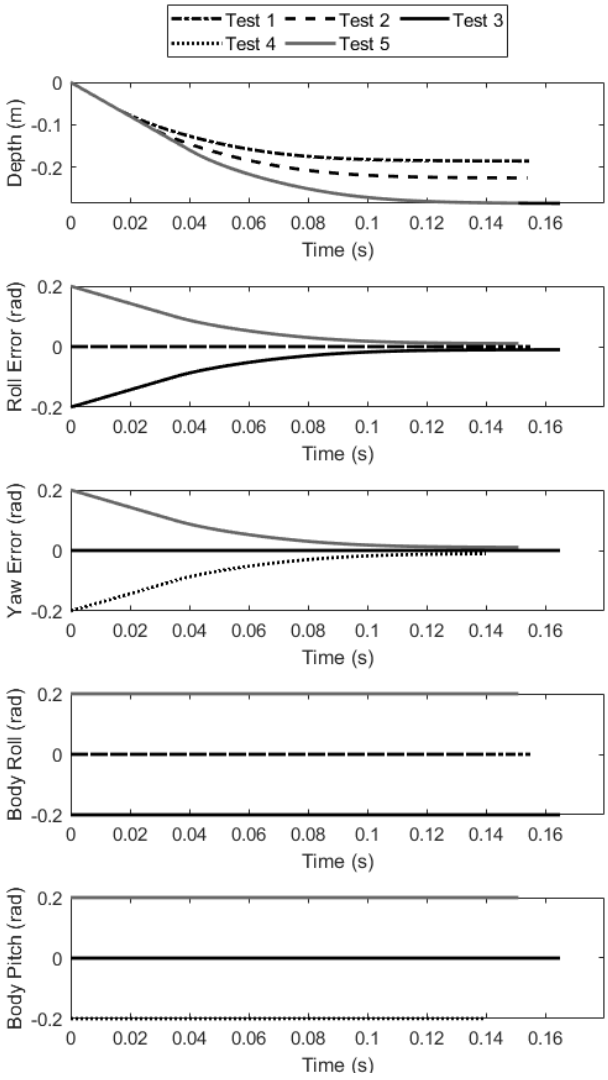

Fig. 11. Parameters and errors versus time.

VI. CONCLUSION

Equations were proposed that expanded on both the track dynamics in [21] and the blade dynamics in [18]. The track forces were broadened to include the forces, moments, and rotation matrices associated with three-dimensional surfaces. The blade forces were expanded to consider non-symmetric three-dimensional mounds in front of the blade and the corresponding moments.

Following from the HDMM, a primary fuzzy blade controller was proposed that actuated the bulldozer blade's yaw, pitch, and roll hydraulics. The inputs into this controller were the difference between the current and desired blade angles. The desired pitch angle was determined using a secondary fuzzy controller whose input was an observed soil type. The output of the secondary controller was a desired cutting depth from which the desired pitch angle was ascertained using the known blade arm length. The other desired blade angles were chosen depending on the needs of each given test. This control scheme was created to mimic how a human operator might go about actuating a bulldozer. Each test saw a smooth transition

into their desired test surfaces. These tests show the potential to perform real-world autonomous maneuvers that have not been demonstrated in the literature to this point.

Future work from the authors will aim to generate 3D real-world maps and deploy the controller(s) proposed in this paper on a real-world bulldozer. Potential future directions include expanding the dynamics to better reflect the internals associated with electric or diesel bulldozers. A more accurate blade model could also be included to enable more subtle control around pile accumulation. Additionally, the model's surface-track transition across surfaces with different slope angles could be fleshed out more.

REFERENCES

[1] A. Schwantes and M. Thompson, "Clearing land with the bulldozer," *Extension Bulletin 212*, 1940.

[2] F. E. Griffith, R. L. Kimball, and M. O. Magnuson, *Demonstration and Evaluation of Five Methods of Secondary Backfilling of Strip-mine Areas*. US Department of the Interior, Bureau of Mines, 1966, vol. 6772.

[3] A. Bulgakov, T. Bock, and G. Tokmakov, "Mechatronic control system for leveling of bulldozer blade," in *ISARC. Proceedings of the International Symposium on Automation and Robotics in Construction*, vol. 37. IAARC Publications, 2020, pp. 552–557.

[4] R. Harrington, "Landscape with bulldozer: machines, modernity and environment in post-war britain," *Histories of technology, the environment and modern Britain*, pp. 41–61, 2018.

[5] K. Ohtsubo and E. D. Ward, "A nonlinear automatic feedback blade controller for improved bulldozer performance," *SAE Transactions*, pp. 2055–2066, 1975.

[6] Y.-S. Lee, S.-H. Kim, J. Seo, J. Han, and C.-S. Han, "Blade control in cartesian space for leveling work by bulldozer," *Automation in Construction*, vol. 118, p. 103264, 2020.

[7] T. Mononen, J. Mattila, and A. Kolu, "Blade control for surface profile tracking by heavy-duty bulldozers," in *Fluid Power Systems Technology*, vol. 85239. American Society of Mechanical Engineers, 2021, p. V001T01A017.

[8] T. Mononen and J. Mattila, "Flow-bounded velocity controller for hydraulic bulldozers," *Energies*, vol. 15, no. 11, p. 4027, 2022.

[9] T. Mononen, A. Kolu, and J. Mattila, "Semi-autonomous bulldozer blade control using real-time terrain mapping," in *2022 IEEE/ASME International Conference on Advanced Intelligent Mechatronics (AIM)*. IEEE, 2022, pp. 775–782.

[10] T. Mononen, M. M. Aref, and J. Mattila, "Nonlinear model predictive control of a heavy-duty hydraulic bulldozer blade," in *2019 IEEE International Conference on Cybernetics and Intelligent Systems (CIS) and IEEE Conference on Robotics, Automation and Mechatronics (RAM)*. IEEE, 2019, pp. 565–570.

[11] K. You, L. Ding, Y. Jiang, Z. Wu, and C. Zhou, "End-to-end deep learning for reverse driving trajectory of autonomous bulldozer," *Knowledge-Based Systems*, vol. 252, p. 109402, 2022.

[12] K. You, L. Ding, Q. Dou, Y. Jiang, Z. Wu, and C. Zhou, "An imitation from observation approach for dozing distance learning in autonomous bulldozer operation," *Advanced Engineering Informatics*, vol. 54, p. 101735, 2022.

[13] R. FUKAGAWA, T. MURO, and T. SUZUKI, "A study on fuzzy control of bulldozer blade," *Doboku Gakkai Ronbunshu*, vol. 1992, no. 444, pp. 77–85, 1992.

[14] T. Terano, S. Masui, and K. Nagaya, "Experimental study of fuzzy control for bulldozer," in *TENCON'92-Technology Enabling Tomorrow*. IEEE, 1992, pp. 644–647.

[15] J. Selech, D. Ulbrich, K. Włodarczyk, Ż. Staszak, J. Marcinkiewicz, D. Romek, and B. Baran, "A working design of a bulldozer blade as additional equipment of a compaction drum roller," in *MATEC Web of Conferences*, vol. 254. EDP Sciences, 2019, p. 04005.

[16] R. Mueller, J. Schuler, A. Nick, A. Wilkinson, C. Gallo, and R. King, "Lightweight bulldozer attachment for construction and excavation on the lunar surface," in *AIAA SPACE 2009 conference & exposition*, 2009, p. 6466.

[17] T. Tsuji, Y. Nakagawa, N. Matsumoto, Y. Kadono, T. Takayama, and T. Tanaka, "3-d dem simulation of cohesive soil-pushing behavior by bulldozer blade," *Journal of Terramechanics*, vol. 49, no. 1, pp. 37–47, 2012.

[18] H. Wang, Y. Huang, A. Khajepour, and Q. Song, "Model predictive control-based energy management strategy for a series hybrid electric tracked vehicle," *Applied Energy*, vol. 182, pp. 105–114, 2016.

[19] B. D. Zhang, X. Zhang, L. Zhang, and L. H. Xi, "Development and validation of a series hybrid electric bulldozer model on whole working condition," *Key Engineering Materials*, vol. 693, pp. 1811–1817, 2016.

[20] Z. Yaojuan, C. Kai, Z. Peng, and W. Zhilin, "Research on the simulation of the driving system of crawler bulldozer," in *Proceedings 2011 International Conference on Transportation, Mechanical, and Electrical Engineering (TMEE)*. IEEE, 2011, pp. 703–706.

[21] N. Strawa, D. I. Ignatyev, A. C. Zolotas, and A. Tsourdos, "On-line learning and updating unmanned tracked vehicle dynamics," *Electronics*, vol. 10, no. 2, p. 187, 2021.

[22] G. G. Slabaugh, "Computing euler angles from a rotation matrix," *Retrieved on August*, vol. 6, no. 2000, pp. 39–63, 1999.

[23] L. Caracciolo, A. de Luca, and S. Iannitti, "Trajectory tracking control of a four-wheel differentially driven mobile robot," in *Proceedings 1999 IEEE International Conference on Robotics and Automation (Cat. No.99CH36288C)*, vol. 4, 1999, pp. 2632–2638 vol.4.

[24] M. Ahmad, V. Polotski, and R. Hurteau, "Path tracking control of tracked vehicles," in *Proceedings 2000 ICRA. Millennium Conference. IEEE International Conference on Robotics and Automation. Symposia Proceedings (Cat. No.00CH37065)*, vol. 3, 2000, pp. 2938–2943 vol.3.

[25] ——, "Path tracking control of tracked vehicles," in *Proceedings 2000 ICRA. Millennium Conference. IEEE International Conference on Robotics and Automation. Symposia Proceedings (Cat. No.00CH37065)*, vol. 3, 2000, pp. 2938–2943 vol.3.

[26] R. A. Serway, *Physics for Scientists & Engineers*, 2nd ed. Saunders Golden Sunburst Series, 1986.

[27] M. A. Johnson and M. H. Moradi, *PID control*. Springer, 2005.

[28] A.-T. Nguyen, T. Taniguchi, L. Eciolaza, V. Campos, R. Palhares, and M. Sugeno, "Fuzzy control systems: Past, present and future," *IEEE Computational Intelligence Magazine*, vol. 14, no. 1, pp. 56–68, 2019.

[29] K. M. Passino, S. Yurkovich, and M. Reinfrank, *Fuzzy control*. Addison-wesley Reading, MA, 1998, vol. 42.

[30] R. R. Yager and D. P. Filev, "Generalizing the modeling of fuzzy logic controllers by parameterized aggregation operators," *Fuzzy Sets and Systems*, vol. 70, no. 2, pp. 303–313, 1995. [Online]. Available: https://www.sciencedirect.com/science/article/pii/016501149400224U

[31] I. Iancu, "A mamdani type fuzzy logic controller," *Fuzzy logic-controls, concepts, theories and applications*, vol. 15, no. 2, pp. 325–350, 2012.

[32] F. A. Valentine, "A lipschitz condition preserving extension for a vector function," *American Journal of Mathematics*, vol. 67, no. 1, pp. 83–93, 1945. [Online]. Available: http://www.jstor.org/stable/2371917

[33] H. Khalil, *Nonlinear Systems*, ser. Pearson Education. Prentice Hall, 2002.

[34] "650 p-tier — dozer — john deere us," https://www.deere.com/en/dozers/small-dozers/650-p-dozer/, accessed: 2024-2-21.

[35] J. Y. Wong, *Theory of ground vehicles*. John Wiley & Sons, 2022.

[36] M. Z. Tekeste, T. R. Way, Z. Syed, and R. L. Schafer, "Modeling soil-bulldozer blade interaction using the discrete element method (dem)," *Journal of Terramechanics*, vol. 88, pp. 41–52, 2020.

[37] H. Wang, Q. Song, S. Feng-Chun, and P. Zeng, "Parameters matching and simulation on a hybrid power system for electric bulldozer," in *2nd International Conference on Electronic & Mechanical Engineering and Information Technology*. Atlantis Press, 2012, pp. 2137–2142.

[38] A. Bulgakov, T. Bock, and G. Tokmakov, "Bulldozer as a mechatronics system with the intelligent control," in *ISARC. Proceedings of the International Symposium on Automation and Robotics in Construction*, vol. 31. IAARC Publications, 2014, p. 1.